roles of NDRG2 in the regulation of different signalling pathways may provide clues in understanding the underlying mechanisms of cancer.

Methods

Cell lines. Jurkat, MOLT4, KAWAI and MKB1 are HTLV-1-negative human T-ALL cell lines. KOB, SO4 and KK1 are IL2-dependent ATLL cell lines. ED, Su9T-01 and S1T are IL2-independent ATLL cell lines. MT2, MT4 and HUT102 are human T-cell lines transformed by HTLV-1 infection. Jurkat, MOLT4 and MKB1 were obtained from the Fujisaki Cell Center, Hayashibara Biochemical Laboratories (Okayama, Japan). KAWAI was kindly provided by Dr Y. Hayashi (Gunma Children's Medical Center, Gunma, Japan). MT2, MT4 and HUT102 were kind gifts from Dr H. Iha (Oita University, Oita, Japan). KOB, SO4 and KK1 were kind gifts from Dr Y. Yamada (Nagasaki University, Nagasaki, Japan). Su9T-01 and S1T were kind gifts from Dr N. Arima (Kagoshima University, Kagoshima, Japan). ED was a kind gift from Dr M. Maeda (Kyoto University, Kyoto, Japan). AML cell lines UCSD/AML1, Kasumi-3, K051, NH and MOLM1 were obtained from Dr R. Taetle (VA Medical Center, Sepulveda, CA, USA), from Dr H. Asoh (Hiroshima University, Hiroshima, Japan), from Dr T. Nomura (Nippon Medical School, Tokyo, Japan), from Dr K. Suzukawa (University of Tsukuba, Ibaraki, Japan) and from the Fujisaki Cell Center, Hayashibara Biochemical Laboratories (Okayama, Japan), respectively, and OIH-1 and FKH-1 were obtained from Dr H. Hamaguchi (Musashino Red Cross Hospital). Pancreatic cancer cell lines KLM1, PK9 and PK45P, OSCC cell lines SAS, HO-1-U-1, Ca9-22, HSC2, HSC3, HSC4, HSQ89 and Sa3, cervical cancer cell line HeLa, human embryonic kidney cell line HEK293T and mouse embryonic fibroblast cell line NIH3T3 were obtained from RIKEN Bioresource Center (Tsukuba, Japan). Hepatic cancer cell lines HLF and HuH28 and breast cancer cell line SK-BR-3 were obtained from the Japanese Cancer Research Resources Bank (Tokyo, Japan). Hepatic cancer cell lines HepG2 and HuH7 were obtained from the Health Science Research Resources Bank (Osaka, Japan). Lung cancer cell lines A549, H322, H1395, H1437 and H1648 were obtained from the American Type Culture Collection (Rockville, MD, USA). Glioblastoma cell line A172 and neuroblastoma cell lines NH6 and NH12 were kind gifts from Dr Y. Hayashi (Gunma Children's Medical Center, Gunma, Japan). Prostate cancer cell line PC3 was a kind gift from Dr T. Ochiya (National Cancer Center Research Institute, Tokyo, Japan). Gastric cancer cell lines Mkb28, Mkb45, and KatoIII and ovarian cancer cell line SKOV3 were kind gifts from Dr H. Kataoka (University of Miyazaki, Miyazaki, Japan). IL2-dependent ATLL cell lines were maintained in RPMI 1640 medium (Wako) supplemented with 10% fetal bovine serum and 50 JRU per ml recombinant human IL2 (Takeda). HTLV-1-negative cell lines, cell lines transformed with HTLV-1 and IL2-independent ATLL cell lines were maintained in the same medium without IL2. The other cell lines were cultured in RPMI 1640 or Dulbecco's modified Eagle's medium (Wako) supplemented with 10% fetal bovine serum.

Patient samples. Blood samples were obtained with informed consent with approval by the Institutional Review Board of the Faculty of Medicine, University of Miyazaki. ATLL cells were collected from the patients at the time of hospital admission before the chemotherapy started. The diagnosis of ATLL was based on clinical features, hematological characteristics and the presence of anti-HTLV-1 antibodies in the sera. Monoclonal HTLV-1 provirus integration into the DNA of leukaemic cells was confirmed by Southern blot analysis in all cases. Peripheral blood mononuclear cells (PBMCs) obtained from healthy volunteers and patients with ATLL were purified by gradient centrifugation (Sigma-Aldrich). The procedure for the isolation of ATLL cells from PBMCs has been described elsewhere[54]. $CD4^+$ T cells were purified from PBMCs of healthy volunteers by using anti-CD4 magnetic beads (Miltenyi Biotec) according to the manufacturer's instructions.

Antibodies and reagents. A synthetic peptide (17-PGQTPEAAKTHSVET-31) of human NDRG2 conjugated to keyhole limpet haemocyanin was used for immunization to generate a rabbit polyclonal antibody against NDRG2 (ref. 55). Mouse monoclonal (M2) and rabbit polyclonal (F7425) antibodies against FLAG, and mouse monoclonal antibody (AC-15) against β-actin were purchased from Sigma-Aldrich. Rabbit monoclonal antibodies against PTEN (138G6), phospho-AKT (Ser473) (D9E), phospho-AKT (Thr308) (244F9), phospho-GSK3β (Ser9) (D85E12), GSK3β (27C10), and PP2A C Subunit (PP2Ac) (52F8), rabbit polyclonal antibodies against phospho-PTEN (Ser380/Thr382/383) (9554), non-phospho-PTEN (Ser380/Thr382/383) (9569), AKT (9272), FOXO1/4 (9462) and cleaved caspase-3 (9661), and mouse monoclonal antibodies against PTEN (26H9) and Myc-tag (9B11) were obtained from Cell Signaling Technology. Rabbit polyclonal antibodies against phospho-PTEN (Ser370) (07-889) and PI3K p85 (06-195) were obtained from Upstate/Millipore, rabbit polyclonal antibody against phospho-PTEN (Ser385) (44-1064G) was obtained from Biosource, mouse monoclonal antibody against SHIP1 (P1C1) and goat polyclonal antibody against NDRG2 (E20) were obtained from Santa Cruz Biotechnology, rabbit polyclonal antibody against GFP (598) was obtained from MBL, and rat monoclonal antibodies against mouse B220 (RA3-6B2), mouse CD4 (RM4-5) and mouse CD8 (53-6.7) and hamster monoclonal antibody against mouse CD3 (500A2) were obtained from BD Pharmingen. Mouse monoclonal antibody against TAX (MI73) was a kind gift from Dr M. Matsuoka (Kyoto University, Kyoto, Japan). Recombinant human PP2A core enzyme made up of polyhistidine-tagged (His_{8X}) human PP2Ac and FLAG-tagged human PR65/A co-expressed in baculovirus-infected High Five cell, OA and trichostatin A were obtained from Wako. Dimethyl 3,3′-dithiobispropionimidate (DTBP) was obtained from Thermo Fisher Scientific, and TBB was obtained from Calbiochem. CX-4945 was obtained from Selleckchem, and 5-aza-2'-deoxycytidine was obtained from Sigma-Aldrich.

Plasmid construction. Full-length complementary DNA (cDNA) of *NDRG2* was isolated by RT–PCR from total RNA of the MOLT4 cell line and subcloned into the p3XFLAG-myc-CMV-26 expression vector (Sigma-Aldrich) by standard cloning procedures (FLAG-NDRG2). The FLAG-tagged NDRG2 deletion constructs—NDRG2-deltaN (amino acids 26–357), NDRG2-deltaC (amino acids 1–304), NDRG2-NDR (amino acids 26–304), NDRG2-HD (amino acids 81–297) and NDRG2-Cterm (amino acids 259–357)—were generated by PCR using the NDRG2/pCMV26 as the template and subcloned into p3XFLAG-myc-CMV-26. The GFP-PTEN constructs—GFP-PTEN, GFP-PTEN-N (amino acids 1–185) and GFP-PTEN-C (amino acids 186–403)—were generated by PCR using the PTEN/pcDNA3 (a kind gift from Dr T. Kohno, National Cancer Center Research Institute, Tokyo, Japan) as the template and subcloned into pEGFP-C1 vector (Clontech). A full-length *PTEN* cDNA was amplified from the Su9T-01 cell line by PCR and subcloned into the p3XFLAG-myc-CMV-26. To generate substitution mutant PTEN expression vectors (PTEN-S370A, -S380A/T382A/T383A and -S385A), PCR-based mutagenesis were performed to introduce mutations in the PTEN coding sequence using mutagenic primers listed in Supplementary Table 8 and p3XFLAG-myc-CMV-26/PTEN plasmid as the template. All PCR-generated products were confirmed by nucleotide sequencing. The expression vector for constitutively active PI3K (pmycBD110)[56], which carries the p110-binding domain of p85α attached to the N-terminal region of p110, was kindly provided by Dr Y. Fukui (National Health Research Institutes, Taiwan). The myc-PP1c/pcDNA3, myc-PP2Ac/pcDNA3 and myc-PP5c/pcDNA3 constructs have been described elsewhere[57].

Bisulfite sequencing. A 200-ng DNA sample was denatured in 0.2 M NaOH followed by the addition of bisulfite solution (2.5 M sodium bisulfite, 10 mM hydroquinone and 240 mM NaOH). The mixture was then incubated at 55 °C for 16 h. DNA samples were desulfonated in 0.2 M NaOH and precipitated with ethanol. PCR was performed in a 20-μl volume containing 1 μl of bisulfite-treated DNA, 500 μM of dNTP and 500 nM of each primer for the *NDRG2* promoter region (nucleotides 20564110-20563790, GenBank accession no. NC_000014) (forward 5′-TTTTCGAGGGGTATAAGGAGAGTTTATTTT-3′ and reverse 5′-CCAAAAACTCTAACTCCTAAATAAACA-3′) (ref. 48), and 1 unit of Taq polymerase (Takara) under the following conditions: 98 °C for 30 s; 40 cycles of 98 °C for 10 s, 60 °C for 5 s and 72 °C for 30 s; and final extension at 72 °C for 3 min. PCR products were subcloned into the pTA2 vector (TOYOBO) and sequenced.

Real-time RT–PCR analysis. Total RNA was isolated from cells using TRIzol reagent (Invitrogen) and 1 μg of total RNA was reverse transcribed to obtain first-strand cDNA using an RNA-PCR kit (Takara) following the manufacturer's instructions. The resulting cDNA was used for real-time RT–PCR using a SYBR Green PCR Master Mix kit (Applied Biosystems). PCR was performed in a 25-μl volume containing 1 μl cDNA, 300 μM of each primer and 12.5 μl of 2 × PCR master mix under the following conditions: 95 °C for 10 min followed by 40 cycles of 95 °C for 15 s and 60 °C for 1 min. For NDRG2 primers, the cycling conditions were 95 °C for 10 min, 40 cycles of 95 °C for 15 s, 60 °C for 20 s and 72 °C for 40 s. The primers used were as follows: for *PTEN*, PTEN-F (5′-CAGCCATCATCAAAGAGATCG-3′) and PTEN-R (5′-TTGTTCCTGTATACGCCTTCAA-3′); for *NDRG2*, NDRG2-F (5′-CTGGAACAGCTACAACAACC-3′), and NDRG2-R (5′-TCAACAGGAGACCTCCATGG-3′); and for β-actin, ACTB-F (5′-GACAGGATGCAGAAGGAGATTACT-3′), and ACTB-R (5′-TGATCCACATCTGCTGGAAGGT-3′). The data were normalized to the amount of β-actin mRNA, and the values are represented as the mean ± s.d. of $2^{-\Delta\Delta Ct}$ in a duplicate assay.

Western blot analysis. Cell lysate samples were prepared in NP-40 lysis buffer (50 mM Tris–HCl, pH 8.0, 150 mM NaCl, 5 mM EDTA, 1% NP-40) supplemented with protease inhibitor cocktail (Sigma-Aldrich) and phosphatase inhibitors (PhosStop, Roche) or by direct lysis in boiling Laemmli SDS sample buffer (62.5 mM Tris–HCl, pH 6.8, 2% SDS, 25% glycerol, 5% β-mercaptoethanol and 0.01% bromophenol blue). Protein samples were electrophoresed on 10% SDS-polyacrylamide gel and transferred to polyvinylidine difluoride membranes (Immobilon-P, Millipore). The membranes were blocked in Tris-buffered saline (TBS)-Tween (0.1%) with either 5% bovine serum albumin (BSA) or 5% nonfat dried milk and were then incubated with each primary antibody diluted in TBS containing 0.1% Tween 20 supplemented with either 5% nonfat dried milk or 5% BSA or in the Can Get Signal buffer (TOYOBO). Bound antibody was detected by a Lumi-light Plus kit according to the manufacturer's instructions (Roche Diagnostics). Band intensities on blots were quantified using NIH Image J software. All primary antibodies were used at a dilution of 1:1,000, except anti-β-actin

(1:5,000) and anti-NDRG2 (E20, 1:250). Representative full-gel bots are provided in the Supplementary Fig. 22)

Immunoprecipitation assays. For detecting interaction between endogenous proteins, MOLT4 cells (1×10^7) and mouse frontal cortex tissue were solubilized with RIPA buffer (50 mM Tris–HCl, pH 7.8, 150 mM NaCl, 1% NP-40, 0.25% sodium deoxycholate and 1 mM EDTA) and NP-40 lysis buffer, respectively, supplemented with protease inhibitor cocktail (Sigma-Aldrich) and phosphatase inhibitors (PhosStop, Roche), and the lysates were then incubated with control rabbit immunoglobulin G or antibodies against NDRG2 (rabbit polyclonal, 1:500 or E20, 1:200) or PTEN (26H9, 1:100 or 138G6, 1:300), plus Protein G beads (Amersham Biosciences). After washing, the bound proteins were subjected to SDS-polyacrylamide gel electrophoresis (SDS-PAGE) and immunoblotting with antibodies against NDRG2 (rabbit polyclonal or E20) or PTEN (26H9 or 138G6). For overexpressed proteins, 293T cells were co-transfected with the indicated constructs using HilyMax (Dojindo) according to the manufacturer's instructions. After culturing for 48 h, the transfected cells were solubilized with RIPA buffer, and the lysates were then subjected to immunoprecipitation using FLAG M2 affinity gel (Sigma-Aldrich) or antibodies against GFP (1:200) or PTEN (138G6, 1:500), followed by immunoblotting with antibodies against either FLAG (F7425), GFP or PTEN (26H9). For chemical crosslinking, stable HUT102 or KK1 cell lines expressing FLAG-NDRG2 were washed twice with phosphate-buffered saline (PBS) and incubated with 2 mM DTBP in PBS at room temperature for 30 min. After washing twice with PBS, cells were lysed in TNT buffer (10 mM Tris–HCl, pH 7.5, 150 mM NaCl and 0.5% Triton X-100) supplemented with protease inhibitor cocktail (Sigma-Aldrich) and phosphatase inhibitors (Halt phosphatase inhibitor cocktail, Thermo Scientific), and the lysates were immunoprecipitated with control rabbit immunoglobulin G, antibody against PTEN (138G6, 1:500), or FLAG M2 affinity gel, followed by immunoblotting with antibodies against FLAG (F7425), PP2Ac, PTEN (138G6) or phospho-PTEN (Ser380/Thr382/Thr383).

Immunofluorescence staining. Cells were fixed with 4% paraformaldehyde for 10 min at room temperature, washed with TBS 0.1 M glycine, treated with 0.2% Triton X-100 and rewashed with TBS 0.1 M glycine. After blocking with 1% BSA in TBS, cells were incubated with primary antibodies against NDRG2 (E20, 1:100), FoxO1/4 (1:200), PTEN (138G6, 1:200) or FLAG (M2, 1:500) overnight at 4 °C. The cells were then washed three times with TBS containing 0.1% Tween 20 and incubated with Alexa Fluor-546 anti-mouse, Alexa Fluor-555 anti-rabbit, Alexa Fluor-488 anti-rabbit or Alexa Fluor-488 anti-goat secondary antibodies (Molecular Probes) at room temperature for 2 h. The coverslips were washed three times with TBS containing 0.1% Tween 20 and then mounted on glass slides using an antifade reagent (Invitrogen). Proteins were visualized using a confocal laser scanning microscope (Leica Microsystems). Nuclei were counterstained with 4′,6-diamidino-2-phenylindole (DAPI; Sigma-Aldrich).

RNAi treatment. DNA-based shRNA expression vector (RNAi-Ready pSIREN-RetroQ-ZsGreen vector, Clontech) and siRNA oligonucleotides were used in gene knockdown experiments. The shRNA target sequences were as follows: for human *NDRG2*, shNDRG2#1 (5′-GGTGGAGAGGGCATATGCA-3′) and shNDRG2#2 (5′-GCGAGTCTGGAACTCTTTCTT-3′); for mouse *NDRG2*, 5′-CCGTGAAGA ACAGTGGTAA-3′. A control shRNA vector targeting luciferase (shLuc) was purchased from Clontech. The PP2Acα siRNA (sc-43509) and control siRNA (6568) were purchased from Santa Cruz Biotechnology and Cell Signaling Technology, respectively. The transfections were performed using the Nucleofector V kit (Amaxa) following the company's protocol.

Cell proliferation assays. Cells were seeded onto 96-well microtiter plates at a density of 5×10^3 per well and cultured for the indicated time periods. Viable cells were counted by the methyl thiazolyl tetrazolium assay using a cell counting kit-8 (Dojindo). For stable transfectant cells, cells were seeded into 25 cm^2 flasks at a density of 1×10^5 ml^{-1}, and proliferation rates were assessed by counting the numbers of viable cells every 24 h using Trypan blue staining.

Dephosphorylation assay for synthetic peptides. The PTEN peptide 373-EPDHYRYSDTTDSDPENE-390 and phosphopeptides with pSer380 (EPDHYR-YpSDTTDSDPENE), pThr382 (EPDHYRYSDpTTDSDPENE), pThr383 (EPDHYRYSDTpTDSDPENE) and pSer380/pThr382/pThr383 (EPDHYR-YpSDpTpTDSDPENE) were obtained from TORAY Research Center (Tokyo, Japan). The release of inorganic phosphates from phosphopeptides was determined using a malachite green assay kit (BIOMOL Green reagent, BIOMOL). Cell extracts from the KK1-NDRG2 stable cell line, NIH3T3 cell line and 293T cell line transiently transfected with mock or Myc-tagged PP1c, PP2Ac or PP5c vectors using HilyMax were prepared by lysing cells in TNT buffer supplemented with protease inhibitor cocktail (Sigma-Aldrich). Endogenous PP2Ac and Myc-tagged PP1c, PP2Ac and PP5c were immunoprecipitated using antibodies against anti-PP2Ac (1:500) and anti-Myc (1:500), respectively. For inhibitor treatment, lysates of KK1-NDRG2 cells were incubated on ice for 30 min in the absence or presence of various concentrations of OA. The total cell lysates, immunoprecipitated samples or 0.5 units of recombinant PP2A were incubated with 100 μM PTEN peptide or phosphopeptides in 10 μl of phophatase assay buffer (20 mM HEPES pH 7.0, 1 mM $MnCl_2$, 8 mM $MgCl_2$, 1 mM dithiothreitol and 100 μg ml^{-1} BSA) at 30 °C for 60 min. The reactions were terminated by the addition of 40 μl of TE buffer (10 mM Tris–HCl, pH 8.0, 1 mM EDTA) and 100 μl of BIOMOL Green reagent, and absorbance at 620 nm was determined after incubation for 20 min at room temperature. The quantity of Pi released (nmoles) was calculated based on a standard curve determined for inorganic phosphate according to the manufacturer's recommendations. All assays were performed in duplicate.

PTEN dephosphorylation assay. The KK1-Mock stable cells were lysed in TNT buffer plus protease inhibitor cocktail (Sigma-Aldrich), and the cell lysates were immunoprecipitated with an antibody against PTEN (138G6, 1:500) and Protein G beads. Immunoprecipitates were washed three times with TNT buffer and twice with phosphatase assay buffer, resuspended in phosphatase assay buffer and incubated with 0.5 units of recombinant PP2A for 60 min at 30 °C. The reaction was stopped by adding SDS sample buffer, and the samples were separated by 10% SDS-PAGE, followed by western blotting with antibodies against PTEN (138G6) or phospho-PTEN (Ser370 or Ser380/Thr382/Thr383).

Generation of *NDRG2* knockout mice. *NDRG2*-deficient mice were generated in the Laboratory for Animal Resources and Genetic Engineering, RIKEN Center for Developmental Biology (accession. no. CDB0768K: http://www.cdb.riken.jp/arg/mutant%20mice%20list.html). For generating a targeting vector, genomic fragments for *NDRG2* were obtained from RP23-109J8 BAC clone (BACPAC Resources). A *lacZ*-pA-*neo*-pA cassette was inserted into exon 2 of the *NDRG2* gene to create the targeting construct. The linearized targeting vector was inserted into TT2 ES cells[58] by electroporation, and G418-resistant clones were screened for homologous recombination by PCR and Southern blot analysis using a 457-bp 5′ fragment as the probe. Targeted ES clones were microinjected into ICR eight-cell stage embryos and transferred into pseudopregnant ICR females (http://www.cdb.riken.jp/arg/Methods.html). The resulting chimeras were bred with C57BL/6 mice, and heterozygous offspring were identified by Southern blot analysis and by PCR using the following two primer pairs: WT allele, F1 (5′-CAAACACCCGA GACTGCCAA-3′)/R (5′-ATTAAACAATAAAGATGTCC-3′); targeted-allele, F2 (5′-GACAGGAGAGGATGAAGGTT-3′)/R. Heterozygous mice were backcrossed with C57BL/6 for two generations and mated in the same generation to obtain homozygous mutants. All animal experiments were approved by the Animal Experiment Review Board of the University of Miyazaki.

Histological analysis. All necropsies and histological examinations were performed on mice at the time of death. Tissues were fixed in 10% buffered formalin solution and embedded in paraffin blocks, and 2-μm-thick sections were prepared. Paraffinized sections were deparaffinized with xylene and rehydrated through a decreasing gradient of ethanol solutions. Slides were stained with hematoxylin and eosin (H&E), coverslipped with mounting medium, and viewed under a light microscope. The slides were scanned with a digital scanner (MIRAX; Carl Zeiss) and viewed with MIRAX software (Carl Zeiss). For immunohistochemistry, the tissue sections were deparaffinized and rehydrated. After microwave treatment for 20 min in citrate buffer pH 6.0 and cooling, endogenous peroxidase activity was blocked in 0.3% hydrogen peroxide in methanol for 30 min. After blocking in 5% skim milk in PBS for 30 min, sections were incubated with antibodies against CD3, CD4, CD8, B220, FLAG or cleaved caspase-3 for 60 min at 37 °C, washed three times with PBS and incubated with horseradish peroxidase-conjugated secondary antibodies for 30 min at 37 °C. The horseradish peroxidase activity was visualized with 3, 3′-diaminobenzidine containing hydrogen peroxide. All primary antibodies were used at 1:200 dilution, except anti-FLAG (1:500) and anti-cleaved caspase-3 (1:100).

Statistical analysis. Bars and markers in the figures represent the mean ± s.d. The two-tailed Student's *t*-test and Mann–Whitney *U*-test were used as appropriate. In the Kaplan–Meier survival analysis, the log-rank test was used for analysis. Fisher's exact analysis was used to determine differences in tumour incidence. Differences were considered significant when the *P* value was <0.05, as indicated in the text.

References

1. Takatsuki, K. *et al.* Clinical diversity in adult T-cell leukemia-lymphoma. *Cancer Res.* **45,** 4644s–4645s (1985).
2. Proietti, F. A., Carneiro-Proietti, A. B., Catalan-Soares, B. C. & Murphy, E. L. Global epidemiology of HTLV-I infection and associated diseases. *Oncogene* **24,** 6058–6068 (2005).
3. Yasunaga, J. & Matsuoka, M. Leukaemogenic mechanism of human T-cell leukaemia virus type I. *Rev. Med. Virol.* **17,** 301–311 (2007).
4. Fukuda, R. *et al.* Alteration of phosphatidylinositol 3-kinase cascade in the multilobulated nuclear formation of adult T cell leukemia/lymphoma (ATLL). *Proc. Natl Acad. Sci. USA* **102,** 15213–15218 (2005).

5. Ikezoe, T. *et al.* Longitudinal inhibition of PI3K/Akt/mTOR signaling by LY294002 and rapamycin induces growth arrest of adult T-cell leukemia cells. *Leuk. Res.* **31,** 673–682 (2007).
6. Li, J. *et al.* PTEN, a putative protein tyrosine phosphatase gene mutated in human brain, breast, and prostate cancer. *Science* **275,** 1943–1947 (1997).
7. Steck, P. A. *et al.* Identification of a candidate tumour suppressor gene, MMAC1, at chromosome 10q23.3 that is mutated in multiple advanced cancers. *Nat. Genet.* **15,** 356–362 (1997).
8. Hollander, M. C., Blumenthal, G. M. & Dennis, P. A. PTEN loss in the continuum of common cancers, rare syndromes and mouse models. *Nat. Rev. Cancer* **11,** 289–301 (2011).
9. Ali, I. U., Schriml, L. M. & Dean, M. Mutational spectra of PTEN/MMAC1 gene: a tumor suppressor with lipid phosphatase activity. *J. Natl Cancer Inst.* **91,** 1922–1932 (1999).
10. Cully, M., You, H., Levine, A. J. & Mak, T. W. Beyond PTEN mutations: the PI3K pathway as an integrator of multiple inputs during tumorigenesis. *Nat. Rev. Cancer* **6,** 184–192 (2006).
11. Song, M. S., Salmena, L. & Pandolfi, P. P. The functions and regulation of the PTEN tumour suppressor. *Nat. Rev. Mol. Cell Biol.* **13,** 283–296 (2012).
12. Trotman, L. C. *et al.* Ubiquitination regulates PTEN nuclear import and tumor suppression. *Cell* **128,** 141–156 (2007).
13. Wang, X. *et al.* NEDD4-1 is a proto-oncogenic ubiquitin ligase for PTEN. *Cell* **128,** 129–139 (2007).
14. Maddika, S. *et al.* WWP2 is an E3 ubiquitin ligase for PTEN. *Nat. Cell Biol.* **13,** 728–733 (2002).
15. Vazquez, F., Ramaswamy, S., Nakamura, N. & Sellers, W. R. Phosphorylation of the PTEN tail regulates protein stability and function. *Mol. Cell Biol.* **20,** 5010–5018 (2000).
16. Vazquez, F. *et al.* Tumor suppressor PTEN acts through dynamic interaction with the plasma membrane. *Proc. Natl Acad. Sci. USA* **103,** 3633–3638 (2006).
17. Odriozola, L., Singh, G., Hoang, T. & Chan, A. M. Regulation of PTEN activity by its carboxyl-terminal autoinhibitory domain. *J. Biol. Chem.* **282,** 23306–23315 (2007).
18. Rahdar, M. *et al.* A phosphorylation-dependent intramolecular interaction regulates the membrane association and activity of the tumor suppressor PTEN. *Proc. Natl Acad. Sci. USA* **106,** 480–485 (2009).
19. Silva, A. *et al.* PTEN posttranslational inactivation and hyperactivation of the PI3K/Akt pathway sustain primary T cell leukemia viability. *J. Clin. Invest.* **118,** 3762–3774 (2008).
20. Yang, Z. *et al.* Reduced expression of PTEN and increased PTEN phosphorylation at residue Ser380 in gastric cancer tissues: A novel mechanism of PTEN inactivation. *Clin. Res. Hepatol. Gastroenterol.* **37,** 72–79 (2013).
21. Torres, J. & Pulido, R. The tumor suppressor PTEN is phosphorylated by the protein kinase CK2 at its C terminus. Implications for PTEN stability to proteasome-mediated degradation. *J. Biol. Chem.* **276,** 993–998 (2001).
22. Hidaka, T. *et al.* Down-regulation of TCF8 is involved in the leukemogenesis of adult T-cell leukemia/lymphoma. *Blood* **112,** 383–393 (2008).
23. Popescu, N. C. Genetic alterations in cancer as a result of breakage at fragile sites. *Cancer Lett.* **192,** 1–17 (2003).
24. Yao, L., Zhang, J. & Liu, X. NDRG2: a Myc-repressed gene involved in cancer and cell stress. *Acta Biochim. Biophys. Sin. (Shanghai)* **40,** 625–635 (2008).
25. Fernandes, S., Iyer, S. & Kerr, W. G. Role of SHIP1 in cancer and mucosal inflammation. *Ann. NY Acad. Sci.* **1280,** 6–10 (2013).
26. Al-Khouri, A. M., Ma, Y., Togo, S. H., Williams, S. & Mustelin, T. Cooperative phosphorylation of the tumor suppressor phosphatase and tensin homologue (PTEN) by casein kinases and glycogen synthase kinase 3beta. *J. Biol. Chem.* **280,** 35195–35202 (2005).
27. Qu, X. *et al.* Characterization and expression of three novel differentiation-related genes belong to the human NDRG gene family. *Mol. Cell. Biochem.* **229,** 35–44 (2002).
28. Bialojan, C. & Takai, A. Inhibitory effect of a marine-sponge toxin, okadaic acid, on protein phosphatases, specificity and kinetics. *Biochem. J.* **256,** 283–290 (1988).
29. Hu, X. L. *et al.* Expression analysis of the NDRG2 gene in mouse embryonic and adult tissues. *Cell Tissue Res.* **325,** 67–76 (2006).
30. Lee, D. C. *et al.* Functional and clinical evidence for NDRG2 as a candidate suppressor of liver cancer metastasis. *Cancer Res.* **68,** 4210–4220 (2008).
31. Chang, X. *et al.* DNA methylation of NDRG2 in gastric cancer and its clinical significance. *Dig. Dis. Sci.* **58,** 715–723 (2013).
32. Furuta, H. *et al.* NDRG2 is a candidate tumor-suppressor for oral squamous-cell carcinoma. *Biochem. Biophys. Res. Commun.* **391,** 1785–1791 (2010).
33. Mavros, A. *et al.* Infrequent genetic alterations of the tumor suppressor gene PTEN/MMAC1 in squamous cell carcinoma of the oral cavity. *J. Oral Pathol. Med.* **31,** 270–276 (2002).
34. Kozaki, K. *et al.* PIK3CA mutation is an oncogenic aberration at advanced stages of oral squamous cell carcinoma. *Cancer Sci.* **97,** 1351–1358 (2006).
35. Leslie, N. R., Batty, I. H., Maccario, H., Davidson, L. & Downes, C. P. Understanding PTEN regulation: PIP2, polarity and protein stability. *Oncogene* **27,** 5464–5476 (2008).
36. Miller, S. J., Lou, D. Y., Seldin, D. C., Lane, W. S. & Neel, B. G. Direct identification of PTEN phosphorylation sites. *FEBS Lett.* **528,** 145–153 (2002).
37. Omori, N. *et al.* Enhanced phosphorylation of PTEN in rat brain after transient middle cerebral artery occlusion. *Brain. Res.* **954,** 317–322 (2002).
38. Ning, K. *et al.* A novel leptin signalling pathway via PTEN inhibition in hypothalamic cell lines and pancreatic beta-cells. *EMBO J.* **25,** 2377–2387 (2006).
39. Maccario, H., Perera, N. M., Davidson, L., Downes, C. P. & Leslie, N. R. PTEN is destabilized by phosphorylation on Thr366. *Biochem. J.* **405,** 439–444 (2007).
40. Wang, L. *et al.* NDRG2 is a new HIF-1 target gene necessary for hypoxia-induced apoptosis in A549 cells. *Cell. Physiol. Biochem.* **21,** 239–250 (2008).
41. Liu, J. *et al.* HIF-1 and NDRG2 contribute to hypoxia-induced radioresistance of cervical cancer Hela cells. *Exp. Cell Res.* **316,** 1985–1993 (2010).
42. Burchfield, J. G. *et al.* Akt mediates insulin-stimulated phosphorylation of Ndrg2: evidence for cross-talk with protein kinase C theta. *J. Biol. Chem.* **279,** 18623–18632 (2004).
43. Murray, J. T. *et al.* Exploitation of KESTREL to identify NDRG family members as physiological substrates for SGK1 and GSK3. *Biochem. J.* **384,** 477–488 (2004).
44. Eichhorn, P. J., Creyghton, M. P. & Bernards, R. Protein phosphatase 2A regulatory subunits and cancer. *Biochim. Biophys. Acta* **1795,** 1–15 (2009).
45. Rodgers, J. T., Vogel, R. O. & Puigserver, P. Clk2 and B56β mediate insulin-regulated assembly of the PP2A phosphatase holoenzyme complex on Akt. *Mol. Cell* **41,** 471–479 (2011).
46. Cheong, J. W. *et al.* Phosphatase and tensin homologue phosphorylation in the C-terminal regulatory domain is frequently observed in acute myeloid leukaemia and associated with poor clinical outcome. *Br. J. Haematol.* **122,** 454–456 (2003).
47. Kovács, K. A. *et al.* Phosphorylation of PTEN (phosphatase and tensin homologue deleted on chromosome ten) protein is enhanced in human fibromyomatous uteri. *J. Steroid Biochem. Mol. Biol* **103,** 196–199 (2007).
48. Lusis, E. A. *et al.* Integrative genomic analysis identifies NDRG2 as a candidate tumor suppressor gene frequently inactivated in clinically aggressive meningioma. *Cancer Res.* **265,** 7121–7126 (2005).
49. Tepel, M. *et al.* Frequent promoter hypermethylation and transcriptional downregulation of the NDRG2 gene at 14q11.2 in primary glioblastoma. *Int. J. Cancer* **123,** 2080–2086 (2008).
50. Piepoli, A. *et al.* Promoter methylation correlates with reduced NDRG2 expression in advanced colon tumour. *BMC Med. Genomics* **2,** doi:10.1186/1755-8794-2-11 (2009).
51. Barreau, O. *et al.* Identification of a CpG island methylator phenotype in adrenocortical carcinomas. *J Clin. Endocrinol. Metab.* **98,** E174–E184 (2013).
52. Kim, A. *et al.* Suppression of NF-kappaB activity by NDRG2 expression attenuates the invasive potential of highly malignant tumor cells. *Carcinogenesis* **30,** 927–936 (2009).
53. Park, Y. *et al.* SOCS1 induced by NDRG2 expression negatively regulates STAT3 activation in breast cancer cells. *Biochem. Biophys. Res. Commun.* **363,** 361–367 (2007).
54. Nakahata, S. *et al.* Clinical significance of CADM1/TSLC1/IgSF4 expression in adult T-cell leukemia/lymphoma. *Leukemia* **26,** 1238–1246 (2012).
55. Mitchelmore, C. *et al.* NDRG2: a novel Alzheimer's disease associated protein. *Neurobiol. Dis.* **16,** 48–58 (2004).
56. Kobayashi, M. *et al.* Expression of a constitutively active phosphatidylinositol 3-kinase induces process formation in rat PC12 cells. Use of Cre/loxP recombination system. *J. Biol. Chem.* **272,** 16089–16092 (1997).
57. Sugiyama, K. *et al.* Aurora-B associated protein phosphatases as negative regulators of kinase activation. *Oncogene* **21,** 3103–3111 (2002).
58. Yagi, T. *et al.* A novel ES cell line, TT2, with high germline-differentiating potency. *Anal. Biochem.* **214,** 70–76 (1993).

Acknowledgements

We thank Y. Motoyoshi, A. Nakatake and I. Morinaga for their technical assistance and N. Ishigami for secretarial assistance. We thank all of the members of the Division of Tumor and Cellular Biochemistry and HTLV-1/ATL Research Facility, University of Miyazaki for helpful discussions and comments. Also, we gratefully thank all of the researchers, who kindly provided us their important cell lines and materials. This work was supported by Grant-in-Aid for Scientific Research on Priority Areas (20012043) from the Ministry of Education, Culture, Sports, Science and Technology (MEXT) of Japan; Research fund from Miyazaki Prefecture Collaboration of Regional Entities for the Advancement of Technological Excellence (60G01-B7002022), Japan Science and Technology Agency (JST); Scientific Research (B) (21390098) (KM); and Young Scientists (B) (23701061 to SN and 23790372 to TI) of Japan Society for the Promotion of Science (JSPS).

Author contributions

S.N., T.I. and K.M. designed the research; S.N., T.I., M.H., N.Y. and Y.A. performed the experiments and analysed the results; P.M., T.T., K.O., N.M. and R.Y. performed the

histopathology; Y.S., K.N., T.T. and M.T. performed the SNP array analysis; T.A. and H.K. generated *NDRG2*-deficient mice; M.H. and K.N. performed the cDNA microarray analysis; K.N. and Y.K. performed the DNA methylation array analysis; K.S. provided patient samples; I.K. Y.A., T.T., A.H., and H.S. edited and commented on the manuscripts; S.N. and K.M. wrote the manuscript; K.M. supervised the project.

Additional information

Accession codes: The gene expression data have been deposited in the Gene Expression Omnibus database under accession code GSE43017.

Supplementary Information accompanies this paper at http://www.nature.com/naturecommunications

Competing financial interests: The authors declare no competing financial interests.

Reprints and permission information is available online at http://npg.nature.com/reprintsandpermissions/

How to cite this article: Nakahata, S. *et al.* Loss of NDRG2 expression activates PI3K-AKT signalling via PTEN phosphorylation in ATLL and other cancers. *Nat. Commun.* 5:3393 doi: 10.1038/ncomms4393 (2014).

Leukemia (2015) **29,** 576–585

www.nature.com/leu

ORIGINAL ARTICLE

Hes1 suppresses acute myeloid leukemia development through FLT3 repression

T Kato[1,2,3], M Sakata-Yanagimoto[1,3], H Nishikii[1], M Ueno[4], Y Miyake[3], Y Yokoyama[1], Y Asabe[3], Y Kamada[3], H Muto[1,3], N Obara[1,3], K Suzukawa[1], Y Hasegawa[1,3], I Kitabayashi[5], K Uchida[6], A Hirao[4], H Yagita[7], R Kageyama[8,9] and S Chiba[1,2,3]

In leukemogenesis, Notch signaling can be up and downregulated in a context-dependent manner. The transcription factor hairy and enhancer of split-1 (*Hes1*) is well-characterized as a downstream target of Notch signaling. *Hes1* encodes a basic helix–loop–helix-type protein, and represses target gene expression. Here, we report that deletion of the *Hes1* gene in mice promotes acute myeloid leukemia (AML) development induced by the MLL–AF9 fusion protein. We then found that Hes1 directly bound to the promoter region of the FMS-like tyrosine kinase 3 *(FLT3)* gene and downregulated the promoter activity. FLT3 was consequently upregulated in MLL–AF9-expressing immortalized and leukemia cells with a *Hes1*- or *RBPJ*-null background. MLL–AF9-expressing *Hes1*-null AML cells showed enhanced proliferation and ERK phosphorylation following FLT3 ligand stimulation. FLT3 inhibition efficiently abrogated proliferation of MLL–AF9-induced *Hes1*-null AML cells. Furthermore, an agonistic anti-Notch2 antibody induced apoptosis of MLL–AF9-induced AML cells in a *Hes1*-wild type but not a *Hes1*-null background. We also accessed two independent databases containing messenger RNA (mRNA) expression profiles and found that the expression level of *FLT3* mRNA was negatively correlated with those of *HES1* in patient AML samples. These observations demonstrate that Hes1 mediates tumor suppressive roles of Notch signaling in AML development, probably by downregulating FLT3 expression.

Leukemia (2015) **29,** 576–585; doi:10.1038/leu.2014.281

INTRODUCTION

The Notch pathway, which is highly conserved from *Drosophila* to mammals, functions in maintenance, proliferation and differentiation of various cell types. In mammals, four receptors (Notch1–4) and five ligands (Jagged1/2, Delta-like 1/3/4) have been identified.[1] Ligand binding initiates proteolytic cleavage of the Notch receptor by γ-secretase, leading to nuclear translocation of the Notch intracellular domain.[2] Notch intracellular domain binds to the transcription factor RBPJ (also known as CSL for CBF-1, Su(H) and Lag2) and forms a transactivation complex, inducing transcription of Notch–RBPJ target genes.[3,4]

Hes1 is a commonly described Notch–RBPJ target gene in blood cells.[5] The *Hes1* gene encodes a basic helix–loop–helix transcription factor that recruits co-repressors of the transducin-like enhancer of split (groucho) family.[6] Through its basic helix–loop–helix domain, Hes1 forms either heterodimers with other basic helix–loop–helix transcription factors or homodimers that bind both to canonical enhancer box (E-Box) or N-box (CACNAG) promoter elements.[7,8]

Many lines of evidence indicate that deregulated Notch signaling functions in initiation, promotion and progression of numerous cancers. Genetic evidence for that role in human cancers was first reported in the case of T-cell acute lymphoblastic leukemia (T-ALL) in which activating *Notch1* mutations occur at a frequency >50%,[9,10] possibly reflecting the indispensable role of Notch signaling in development of early T lymphocytes.[11] Subsequently, activating mutations in *Notch1* were identified in mature B-cell neoplasms, including chronic lymphocytic leukemia[12] and mantle cell lymphoma,[13] and in *Notch2* in diffuse large B-cell lymphoma[14] and splenic marginal zone B-cell lymphoma.[15] Gain of function mutations in *Notch* genes have also been identified in non-hematologic malignancies such as breast cancer.[16]

In contrast, mouse genetic studies demonstrate that Notch signaling has tumor suppressive activity in skin[17] and vascular[18] tumors. And, in contrast with genetic evidence gathered from analysis of T-ALL, chronic lymphocytic leukemia and some B-cell lymphomas, Notch signaling reportedly has a tumor-suppressive role in B-cell ALL.[19]

Both pro- and anti-tumorigenic roles of Notch signaling have been reported in myeloid malignancies (Supplementary Table 1). In mouse chronic myeloid leukemia models, myeloid blast crisis transition is facilitated by upregulation of Hes1,[20,21] an event reportedly triggered by expression of the RNA binding protein Musashi2 through downregulation of Numb, an inhibitor of Notch signaling.[21] Subsequently, loss-of-function mutations in multiple components of the Notch pathway, including *Notch2,* have been identified in chronic myelomonocytic leukemia patients.[22] Relevant to acute myeloid leukemia (AML), recent studies also suggest a tumor-suppressive activity: activation of Notch signaling induces apoptosis in human AML cells *in vitro,* and constitutively

[1]Department of Hematology, Faculty of Medicine, University of Tsukuba, Tsukuba, Japan; [2]Life Science center of Tsukuba Advanced Research Alliance, University of Tsukuba, Tsukuba, Japan; [3]Department of Hematology, Graduate School of Comprehensive Human Sciences, University of Tsukuba, Tsukuba, Japan; [4]Division of Molecular Genetics, Cancer and Stem Cell Research Program, Cancer Research Institute, Kanazawa University, Kanazawa, Japan; [5]Molecular Oncology Division, National Cancer Center Research Institute, Tokyo, Japan; [6]Department of Molecular Biological Oncology, Faculty of Medicine, University of Tsukuba, Tsukuba, Japan; [7]Department of Immunology, Juntendo University School of Medicine, Tokyo, Japan; [8]Institute of Virus Research, Kyoto University, Kyoto, Japan and [9]World Premier International Research Initiative-Institute for Integrated Cell-Material Sciences (WPI-iCeMS), Kyoto University, Kyoto, Japan. Correspondence: Professor S Chiba, Department of Hematology, Faculty of Medicine, University of Tsukuba, 1-1-1, Tennodai, Tsukuba 305-8575, Japan.
E-mail: schiba-t@md.tsukuba.ac.jp
Received 13 January 2014; revised 25 August 2014; accepted 9 September 2014; accepted article preview online 19 September 2014; advance online publication, 17 October 2014

active forms of Notch1 and Notch2 reduce leukemogenicity in transgenic mouse models.[23,24]

In this paper, we took advantage of an MLL–AF9-induced AML model in *RBPJ*-deficient mice to confirm that Notch signaling functions as a tumor suppressor in AML. We also conducted experiments with the MLL–AF9-induced AML model in *Hes1*-null mice and demonstrated that Hes1 is indispensable for AML suppression. Finally, we provide evidence that FMS-like tyrosine kinase 3 (FLT3) tyrosine kinase signaling is hyperactivated in *Hes1*-null AML cells. These studies identify Hes1 as the Notch effector functioning to suppress AML development and suggest that loss of *Hes1* promotes oncogenesis through FLT3 upregulation.

MATERIALS AND METHODS

Gene expression analysis

RNA was isolated from MLL–AF9-induced AML cells using an RNeasy kit (QIAGEN, Valencia, CA, USA), and complementary DNA was synthesized with SuperScript III (Invitrogen, Carlsbad, CA, USA). Gene expression analysis was performed on the Mouse Genome 430 2.0 Array (Affymetrix, Santa Clara, CA, USA). The data were analyzed with the Expression Console using Affymetrix default analysis settings and normalized with the Gene Level-RMA Sketch. We used a cutoff level of twofold for both up and downregulation in MLL–AF9/*Hes1*$^{-/-}$ AML cells compared with MLL–AF9/*Hes1*$^{+/+}$ AML cells, and sorted the genes by the relative values. See Supplementary Experimental Procedures for details of sample preparation.

Lentivirus production and generation of stable cell lines

For lentivirus production, HEK293T cells were transfected with the CS–Hes1 or mock plasmid together with the psPAX2 packaging plasmid and the pMD2.G envelope plasmid, and the concentrated supernatant was used to infect THP1 cells. To establish stable lines inducibly expressing Hes1, green fluorescent protein (GFP)-expressing THP1 cells were sorted on a FACSAria (BD Biosciences, San Jose, CA, USA).

Chromatin immunoprecipitation

Detailed protocols for chromatin immunoprecipitation are described in Supplementary Methods. Immunoprecipitated DNA fragments were quantified by real-time PCR with the use of two Flt3 promoter sets, N1 and N2, which amplify sequences including putative Hes1 binding sites, N-boxes (N1, 5′-CACTAG-3′ fragment at position −50/−45 and N2, 5′-CACCAG-3′ fragment at position −425/−419; Supplementary Table 3).

Statistics

Survival of transplanted mice was analyzed statistically using the log-rank test. Correlation of messenger RNA (mRNA) expression levels was statistically evaluated by calculating Pearson's correlation coefficient. Other data were analyzed by using Student's *t*-test. *P*-values < 0.05 were considered significant.

Study approval

All experiments were performed according to NIH guidelines and approved by the University of Tsukuba's Committee on Use and Care of Animals.

Other experimental methods

Mice, transplantation, vectors, flow cytometry, preparation of recombinant retroviruses, cell cycle analysis, apoptosis activity, reverse transcription and real time PCR analysis, reporter assay, short interfering RNA interference, CRISPR-Cas9 system and immunoblotting protocols are described in Supplementary Information.

RESULTS

RBPJ deletion accelerates MLL–AF9-induced leukemia development in mice

To determine whether Notch signaling has a tumor-suppressive function in MLL–AF9-induced AML, we transformed common myeloid progenitors (CMPs) purified from bone marrow of *RBPJ*$^{f/f}$ mice[25,26] by retroviral transduction of a construct containing MLL–AF9–IRES–GFP. To eliminate the *RBPJ* allele in these cells, we serially infected MLL–AF9-transduced *RBPJ*$^{f/f}$ cells with Cre recombinase (iCre)–IRES-nerve growth factor receptor (Supplementary Figure 1A, See Methods). Deletion of the *RBPJ* locus in double-positive RBPJ$^{f/f}$ (MLL–AF9/iCre/*RBPJ*$^{f/f}$) cells was confirmed by genomic PCR (Supplementary Figure 1B). We found that levels of mRNA transcripts encoding *Hes1* and *Hes5* were decreased in MLL–AF9/iCre/*RBPJ*$^{f/f}$ compared with control cells (Figure 1a). MLL–AF9/iCre/*RBPJ*$^{f/f}$ cells proliferated more rapidly than did MLL–AF9/mock/RBPJ$^{f/f}$ cells *in vitro* in the presence

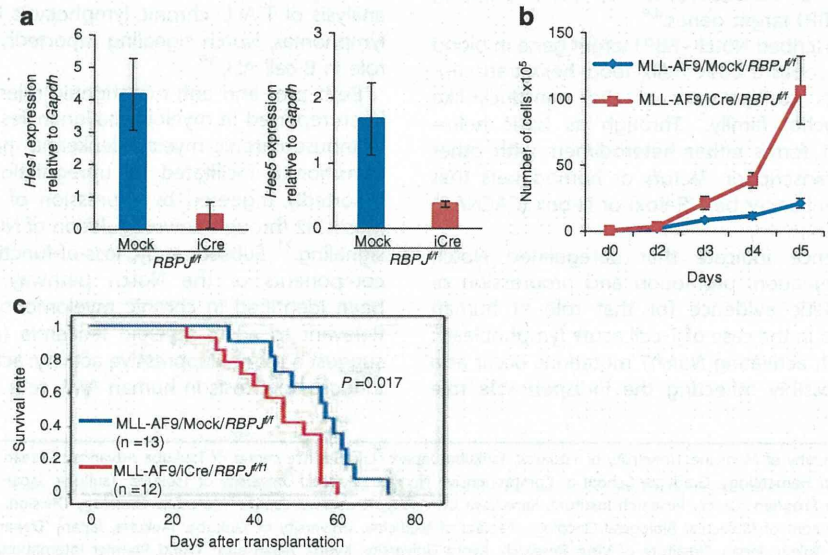

Figure 1. Deletion of *RBPJ* accelerates MLL–AF9-induced leukemia development. (**a**) *Hes1* and *Hes5* transcript levels in MLL–AF9/mock/*RBPJ*$^{f/f}$ and MLL–AF9/iCre/*RBPJ*$^{f/f}$ cells. (**b**) Growth of MLL–AF9/iCre-*RBPJ*$^{f/f}$ and MLL–AF9/mock-*RBPJ*$^{f/f}$ cells cultured in RPMI supplemented with 10% fetal calf serum and interleukin 3. About 50 000 cells were originally plated. Representative data from four independent experiments is shown; $n = 3$ each. (**c**) Survival of mice transplanted with MLL–AF9/iCre/*RBPJ*$^{f/f}$ or MLL–AF9/mock/*RBPJ*$^{f/f}$ cells.

of interleukin 3 (Figure 1b). These results indicate successful knockout of the *RBPJ* locus in MLL–AF9-transduced cells and consequent abrogation of Notch signaling, an outcome that increased proliferation of MLL–AF9-transduced cells.

After deletion of *RBPJ* locus and following expansion of cells for 2–3 weeks in the presence of interleukin 3, MLL–AF9/iCre/*RBPJ*$^{f/f}$ and control cells exhibited a similar myelomonoblastic morphology and surface antigen expression profile (Mac1^{+}, Gr1^{+}, c-Kit$^{+/-}$, Sca1^{-}, CD34$^{+/-}$, B220^{-} and CD3ε^{-}; Supplementary Figure 1C). We then transplanted lethally irradiated syngenic mice through the tail vein with these cells. Mice transplanted with MLL–AF9/iCre/*RBPJ*$^{f/f}$ cells developed leukemia at shorter latencies than did recipients of MLL–AF9/mock/*RBPJ*$^{f/f}$ control cells ($P=0.017$, Figure 1c). In both groups, leukemic cells were found in peripheral blood, bone marrow, spleen, lungs and liver, and no differences in morphology were seen between groups (Supplementary Figures 1D and E).

To exclude the possibility that shortened latency of leukemia development seen following transplantation of MLL–AF9/iCre/*RBPJ*$^{f/f}$ cells was attributable to enhanced homing ability, we compared frequencies of GFP-positive cells in bone marrow 72 h after transplantation. We observed no significant difference in GFP-positive cell frequencies between MLL–AF9/iCre/*RBPJ*$^{f/f}$ and control cells (Supplementary Figure 1F), suggesting that shortened latencies for AML development were due to mechanisms other than enhanced homing ability of *in vitro* expanded MLL–AF9/iCre/*RBPJ*$^{f/f}$ cells. These results indicate that loss of Notch signaling causes enhanced leukemia development from MLL–AF9-transduced cells in mice.

Hes1 loss increases clonogenic potential of MLL–AF9-trandsduced fetal liver CMPs and accelerates development of MLL–AF9-induced leukemia

Hes1 is the best characterized target of the canonical Notch–RBPJ pathway in diverse cellular contexts. To determine if Hes1 was responsible for Notch signaling-mediated suppression of AML development, we employed conventional *Hes1*$^{-/-}$ mice. Although Hes1 is known to repress Hes5 in a certain context,[27] we found *Hes5* expression level was unchanged in this model (data not shown). These mice die at embryonic day (E) 18–19 from defects in neurogenesis.[28] Therefore, we used CMPs prepared from fetal liver at E14.5–15.5. CMPs were retrovirally transduced with MLL–AF9–GFP, and GFP-positive cells were then serially plated in semisolid medium every 7 days. MLL–AF9-transduced CMPs formed colonies at multiple rounds of plating in both *Hes1*-null and wild-type backgrounds. At the second and third replating, colony numbers of MLL–AF9-transduced cells in a *Hes1*-null background (MLL–AF9/*Hes1*$^{-/-}$) were greater than those in a similarly-transduced wild-type (MLL–AF9/*Hes1*$^{+/+}$) background (Supplementary Figure 2A). These results indicate that *Hes1* loss accelerates MLL–AF9-transduced cell proliferation (Figure 2a).

Following the second replating, we expanded MLL–AF9/*Hes1*$^{-/-}$ and MLL–AF9/*Hes1*$^{+/+}$ cells in liquid culture and transplanted them into lethally irradiated syngenic mice. As anticipated, mice transplanted with MLL–AF9/*Hes1*$^{+/+}$ cells developed leukemia at a median latency of 81 days.[29] By comparison, mice transplanted with MLL–AF9/*Hes1*$^{-/-}$ cells developed leukemia at significantly shorter latencies ($P<0.01$, Figure 2b). Leukemia cells with both genotypes were transplantable to the secondary recipients that received sublethal irradiation (data not shown). We compared the *MLL–AF9* mRNA expression levels between AML cells with *Hes1*$^{-/-}$ and *Hes1*$^{+/+}$ genotype, and found no difference (Supplementary Figure 2B). The morphology and cell surface antigen profiles of MLL–AF9/*Hes1*$^{-/-}$ and MLL–AF9/*Hes1*$^{+/+}$ AML cells were essentially the same and similar to those seen in *RBPJ*-deficient AML cells (Supplementary Figures 2C–F).

A previous study suggested that Hes1 downregulate *Bcl2* in AML cells, indicating that *Bcl2* downregulation participates in Notch-induced apoptosis of AML cells.[24] Consistent with this report, the *Bcl2* expression levels were upregulated in MLL–AF9/*Hes1*$^{-/-}$ AML cells compared with MLL–AF9/*Hes1*$^{+/+}$ AML cells (Supplementary Figure 2G).

Taken together, all these results suggest that Hes1 functions downstream to Notch signaling for the suppression of AML development in mice.

Expression of a dominant-negative Hes1 construct enhances AML development

Next, we constructed a dominant-negative mutant of Hes1 (dnHes1) lacking the WRPW domain, which interacts with the transducin-like enhancer co-repressor[30,31] (Figure 3a) and is essential for transcriptional repression. Adult bone marrow CMPs purified from wild-type mice were transformed by retroviral transduction of MLL–AF9–GFP and then serially infected with retrovirus expressing dnHes1–humanized Kusabira Orange (hKO) or mock-hKO. We then sorted both MLL–AF9–GFP/dnHes1–hKO double-positive (MLL–AF9/dnHes1) and control MLL–AF9–GFP/mock-hKO double-positive (MLL–AF9/mock) cells and transplanted them into lethally irradiated mice (Supplementary Figure 3A). Mice harboring MLL–AF9/dnHes1 cells developed leukemia at significantly shorter latencies than did those transplanted with MLL–AF9/mock cells ($P<0.01$, Figure 3b). The morphology of MLL–AF9/dnHes1-induced AML cells was similar to that of MLL–AF9/iCre/*RBPJ*$^{f/f}$- and MLL–AF9/*Hes1*$^{-/-}$-induced AML cells. Cell surface antigen profiles were also similar between these MLL–AF9-induced AML cells, although we observed higher expression levels of CD34 in MLL–AF9/dnHes1-induced AML cells than others (Supplementary Figures 3B and C). This might be

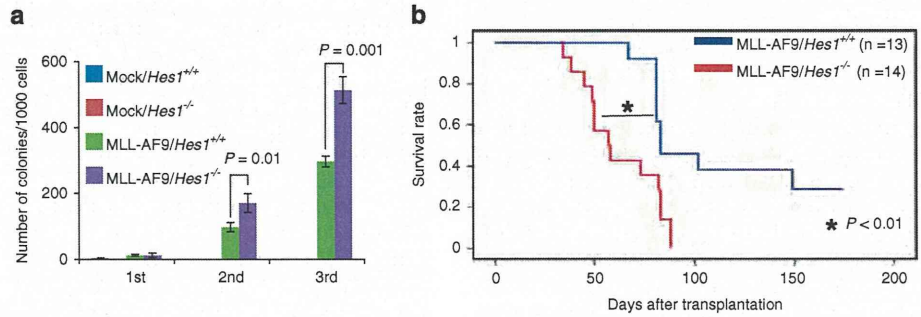

Figure 2. Loss of *Hes1* increases clonogenic potential of MLL–AF9-trandsduced fetal liver CMPs and accelerates development of MLL–AF9-induced leukemia. (**a**) The number of colonies derived from MLL–AF9/*Hes1*$^{-/-}$ cells and MLL–AF9/*Hes1*$^{+/+}$ cells. All cells were harvested, and 1000 cells were replated every 7 days. (**b**) Survival of mice transplanted with MLL–AF9/*Hes1*$^{+/+}$ or MLL–AF9/*Hes1*$^{-/-}$ cells.

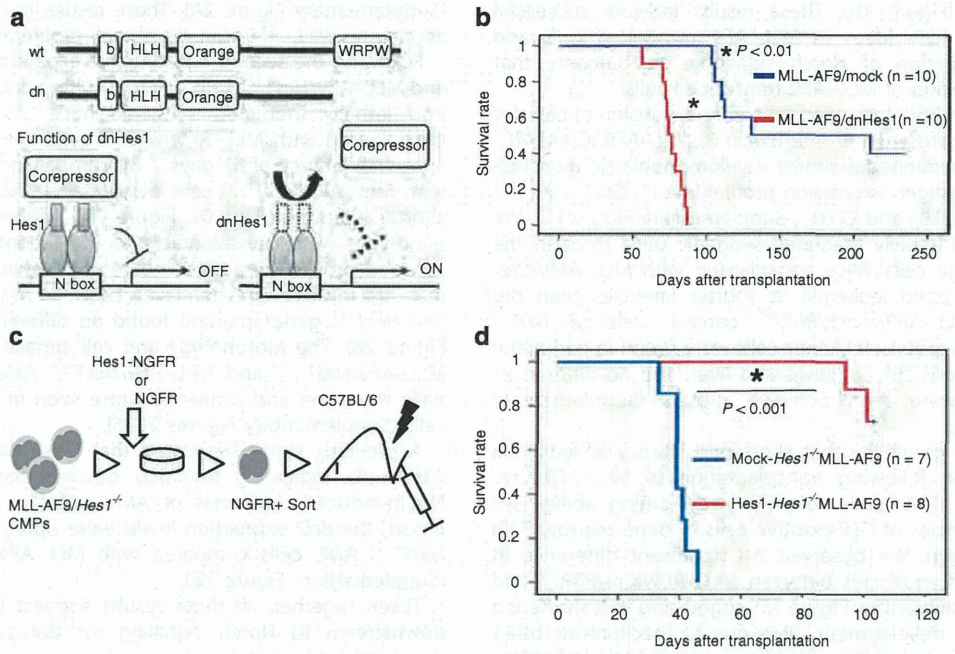

Figure 3. Dominant-negative Hes1 accelerates MLL–AF9-induced leukemia development and re-introduction of wild-type Hes1 into *Hes1*-deficient AML cells represses AML development. (**a**) Structure of the dominant-negative mutant of Hes1 (dnHes1). bHLH, basic helix–loop–helix domain; dn, dominant-negative Hes1; orange, orange domain; WRPW, WRPW motif; WT, wild-type Hes1. (**b**) Survival of mice transplanted with MLL–AF9/dnHes1 or MLL–AF9/mock cells. (**c**) MLL–AF9/*Hes1*$^{-/-}$ cells were serially infected with Hes1-nerve growth factor receptor (Hes1-NGFR). NGFR-positive (Hes1/MLL–AF9/*Hes1*$^{-/-}$) and control (mock/MLL–AF9/*Hes1*$^{-/-}$) cells were sorted and injected into lethally irradiated mice. (**d**) Survival of mice transplanted with Hes1-transduced MLL–AF9/*Hes1*$^{-/-}$ and mock-transduced MLL–AF9/*Hes1*$^{-/-}$ cells.

reflected by the interference with the formation of heterodimers comprising Hes1 and basic helix–loop–helix proteins independent of Notch signaling. MLL–AF9/dnHes1-induced AML cells developed in the primary recipient mice were transplantable to the secondary recipients, which were sublethally irradiated (Data not shown). These findings provide further support that Hes1 is indeed the Notch effector that functions to suppress AML development in this context.

Re-induction of wild-type Hes1 rescues shortened latency of AML development seen in MLL–AF9/*Hes1*$^{-/-}$ cells

To determine whether shortened latency of AML phenotypes in MLL–AF9/*Hes1*$^{-/-}$ cells could be reversed, we reintroduced Hes1 into these cells (Figure 3c). Lethally irradiated mice transplanted with Hes1-transduced MLL–AF9/*Hes1*$^{-/-}$ cells developed leukemia at longer latencies than did mock-transduced MLL–AF9/*Hes1*$^{-/-}$ cells ($P < 0.01$, Figure 3d). These phenotypes indicate that aberrations seen following *Hes1* deletion were reverted by the exogenous expression of Hes1.

Hyperactivation of FLT3 signaling underlies enhanced proliferation of *RBPJ*- and *Hes1*-deficient AML cells

To elucidate signaling downstream of the Notch–RBPJ–Hes1 axis in AML cells, we compared mRNA expression profiles between MLL–AF9/*Hes1*$^{-/-}$ and MLL–AF9/*Hes1*$^{+/+}$ AML cells using microarray analysis (www.ncbi.nlm.nih.gov/geo, accession number GSE50234). Using a cutoff level of twofold, of 35 079 genes, 552 and 376 were up and downregulated, respectively, in MLL–AF9/*Hes1*$^{-/-}$ AML cells compared with control cells (Figure 4a). Among upregulated genes, we focused on *Flt3*, which encodes a receptor-type tyrosine kinase, because hyperactivation of FLT3 signaling by internal tandem duplication mutations or mRNA overexpression is a known indicator of poor prognosis of AML.[32,33] Upregulation of *Flt3* mRNA was validated by quantitative reverse transcription-PCR in both MLL–AF9/*Hes1*$^{-/-}$ cells maintained in liquid culture (data not shown) and in cells recovered from mice that developed AML (Figure 4b). *Flt3* mRNA was also upregulated in MLL–AF9/iCre/*RBPJ*$^{f/f}$ cells and cells expressing dnHes1 (Supplementary Figure 4A). Cell surface FLT3 expression was also higher in MLL–AF9/*Hes1*$^{-/-}$ cells compared with respective controls (Figure 4c). Expression levels of *Flt3* mRNA and cell surface FLT3 protein in Hes1-transduced MLL–AF9/*Hes1*$^{-/-}$ cells decreased relative to those seen in mock-transduced MLL–AF9/*Hes1*$^{-/-}$ cells, and the proliferative capacity of Hes1-transduced MLL–AF9/*Hes1*$^{-/-}$ cells in the presence of FLT3 ligand was lower than that observed in mock-transduced cells (Figure 4d, Supplementary Figures 4B and C). There are two N-boxes on the Flt3 promoter region. We performed chromatin immunoprecipitation assay using a human AML cell line, THP1, in which Hes1 was expressed in an inducible manner with doxycycline, and showed that Hes1 directly bound to the Flt3 promoter region (Figure 4e). We also performed reporter assay, and showed that Hes1, but not dnHes1, repressed the Flt3 promoter activity (Figure 4f). When N-box sites on Flt3 promoter were mutated, repression of the Flt3 promoter activity by Hes1 was mitigated (Figure 4f). Furthermore, FLT3 was phosphorylated following stimulation with FLT3 ligand specifically in MLL–AF9/*Hes1*$^{-/-}$ cells (Figure 4g). Stimulation of cells expressing wild-type FLT3 with FLT3 ligand activates ERK signaling,[34] while signaling through FLT3-internal tandem duplication mutants aberrantly activates other downstream signaling pathways, such as STAT and AKT, in addition to ERK. In MLL–AF9/*Hes1*$^{-/-}$ leukemic cells, ERK phosphorylation was enhanced by FLT3 ligand stimulation, an effect much weakly seen in MLL–AF9/*Hes1*$^{+/+}$ cells (Figure 4g). We did not detect differences in phosphorylation of STAT or AKT in MLL–AF9/*Hes1*$^{-/-}$ and MLL–AF9/*Hes1*$^{+/+}$ leukemic cells (Figure 4g). These results suggest that FLT3–ERK signaling is activated through FLT3 upregulation specifically in the absence of Hes1.

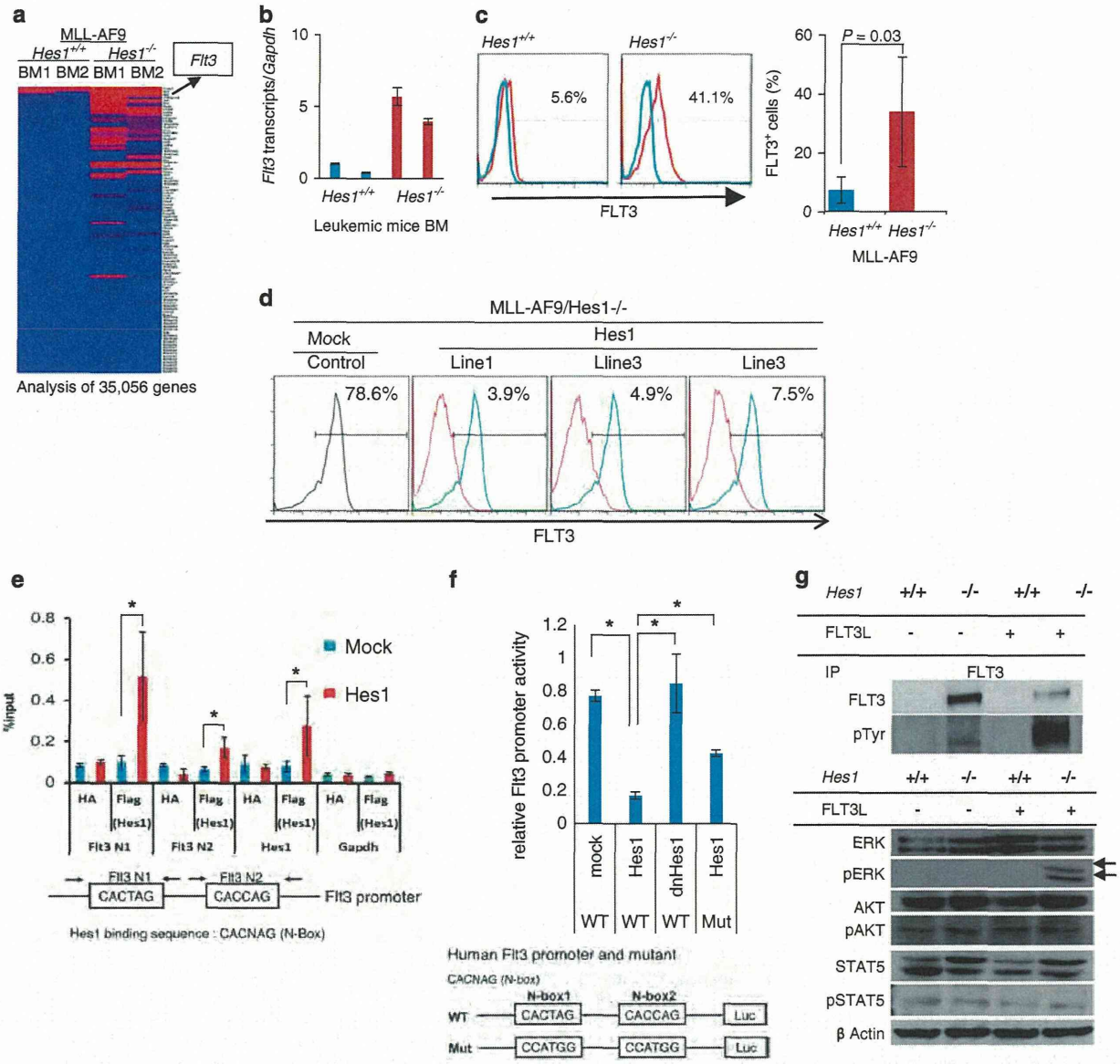

Figure 4. Activation of FLT3 signaling underlies enhanced proliferation of *RBPJ*- and *Hes1*-deficient AML cells. (**a**) Microarray analysis of leukemic bone marrow cells from mice transplanted with MLL–AF9/*Hes1*$^{+/+}$ or MLL–AF9/*Hes1*$^{-/-}$ cells. The colors represent the absolute expression levels. (**b**) *Flt3* transcript levels in leukemic bone marrow cells. Cells were prepared from two mice of each genotype. (**c**) Cell-surface FLT3 expression of leukemic BM cells. Representative histograms are shown (left). (**d**) Cell-surface FLT3 expression of Hes1- or mock-transduced MLL–AF9/*Hes1*$^{-/-}$ cells after serum starvation. (**e**) Chromatin immunoprecipitation analysis for Flag–Hes1 or mock-expressing THP1 cells that used the indicated antibodies ($n = 3$). Error bars indicate ± s.d.; *$P < 0.05$. (**f**) Relative luciferase activity of Flt3 promoter and its N-box mutant in HEK293T cells expressing wild-type Hes1 or dnHes1 protein. Error bars indicate ± s.d.; *$P < 0.05$. A representative result from three independent experiments is shown. Mut, N-box mutants on Flt3 promoter; WT, wild type. (**g**) FLT3 total protein levels and levels of phosphorylated FLT3. MLL–AF9/*Hes1*$^{+/+}$ and MLL–AF9/*Hes1*$^{-/-}$ cells were treated with or without FLT3 ligand. Cell lysates were prepared and immunoprecipitated with anti-FLT3 antibody and then immunoblotted with anti-FLT3 or anti-phosphotyrosine antibodies (4G10).

MLL–AF9/*Hes1*$^{-/-}$ cells, but not MLL–AF9/*Hes1*$^{+/+}$ cells, showed higher proliferative capacity by the FLT3 ligand stimulation than did without this cytokine stimulation (Figure 5a). This effect was blocked by treatment of cells with the FLT3 tyrosine kinase inhibitor KRN383 (ref. 35; Figures 5b and c). Similarly, stimulation of MLL–AF9/iCre/*RBPJ*$^{f/f}$ cells with FLT3 ligand enhanced their proliferation (data not shown), while treatment of these cells with KRN383 in the presence of FLT3 ligand reversed this proliferative effect (Supplementary Figure 4D). Flt3 ligand also increased the number of colonies derived from MLL–AF9/*Hes1*$^{-/-}$ cells, but not MLL–AF9/*Hes1*$^{+/+}$ cells. In contrast, an FLT3 kinase inhibitor, AC220, reduced the number of colonies derived from MLL–AF9/*Hes1*$^{-/-}$cells with or without Flt3 ligand to the level comparable to the number of colonies derived from wild-type cells (Figure 5d). The Flt3 inhibitor did not affect the number of colonies derived from MLL–AF9/*Hes1*$^{+/+}$ cells (Figure 5d). These data indicate that there is a weak autocrine loop for FLT3 signaling, surrounding colonies. The increase in the colony number with MLL–AF9/*Hes1*$^{-/-}$ cells in the second and tertiary platings without exogenous FLT3 ligand shown in Figure 2a, therefore, implies the combinatorial effect of exogenous interleukin 3 and autocrine FLT3 signaling in Hes1-null background.

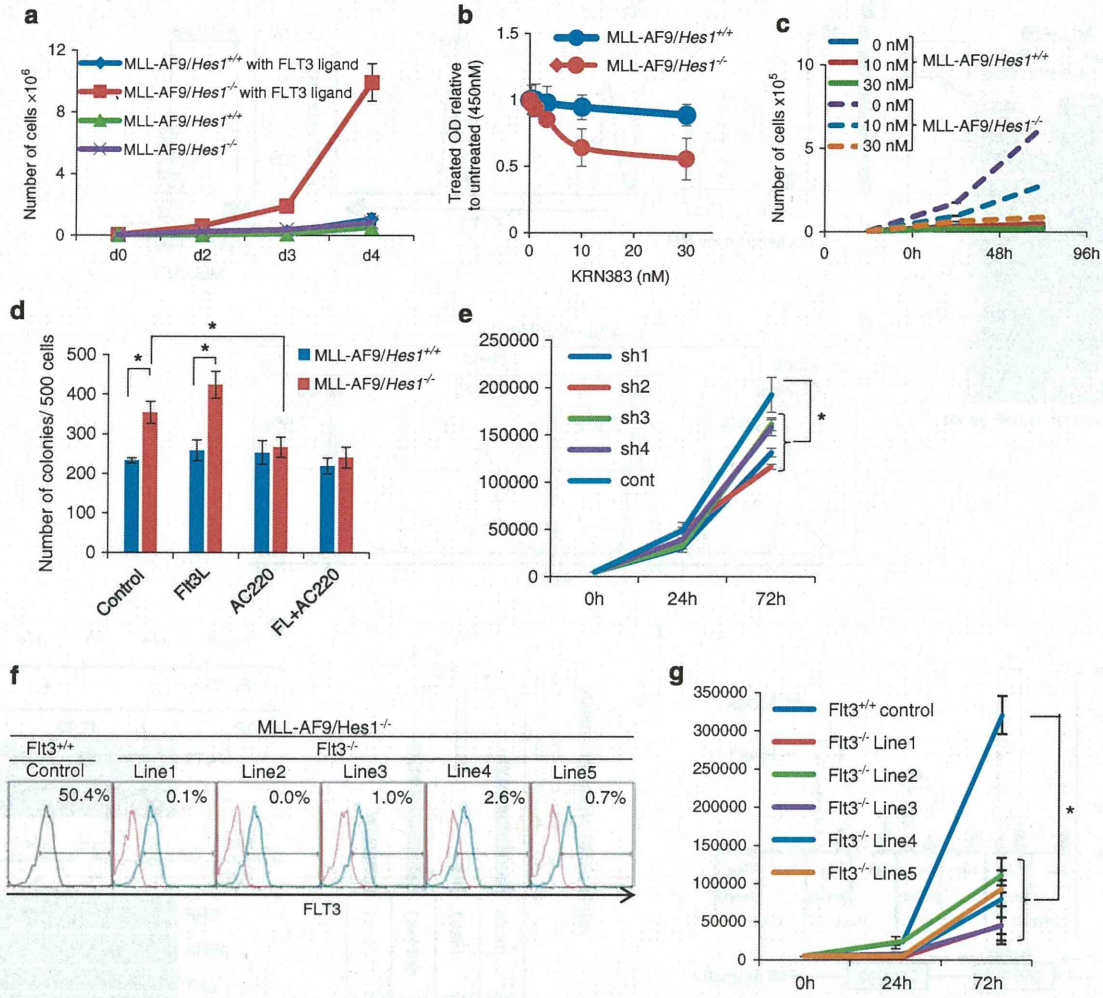

Figure 5. Upregulated FLT3 is biologically functional. (**a**) Growth of MLL–AF9/*Hes1*$^{-/-}$ or MLL–AF9/*Hes1*$^{+/+}$ cells with or without FLT3 ligand in liquid medium containing low interleukin 3 (IL3) levels. Shown are representative results ($n=3$ each). (**b**) Effect of KRN383 on cell viability. MLL–AF9/*Hes1*$^{+/+}$ or MLL–AF9/*Hes1*$^{-/-}$ cells were incubated with 10% fetal calf serum and IL3 containing KRN383 at indicated concentrations. A fractional growth referenced to untreated controls at 48 h is shown. The line represents a fit of data to the Hill equation. (**c**) Growth of MLL–AF9/*Hes1*$^{+/+}$ or MLL–AF9/*Hes1*$^{-/-}$ cells in liquid medium in the presence of KRN383. (**d**) The number of colonies derived from MLL–AF9/*Hes1*$^{-/-}$ and MLL–AF9/*Hes1*$^{+/+}$ cells using either FLT3 ligand or AC220 (FLT3 kinase inhibitor) or both. Error bars indicate ±s.d.; $^{*}P<0.05$. (**e**) Growth of MLL–AF9/*Hes1*$^{-/-}$ cells introduced with shRNA for *Flt3*. Representative data from four independent experiments is shown. $n=4$ each. (**f**) Cell-surface FLT3 expression of *Flt3*-deleted MLL–AF9/*Hes1*$^{-/-}$ cells by CRISPR-Cas9. Blue line, Flt3$^{+/+}$ control cells; Red line, Flt3$^{-/-}$ cells. (**g**) Growth of MLL–AF9/*Hes1*$^{-/-}$ cells with deleted *Flt3* by CRISPR/CAS9. Representative data from three independent experiments is shown; $n=4$ each.

Then, we performed *Flt3* knockdown experiments using short hairpin RNA (shRNA; Supplementary Figure 4E). The growth of the cells introduced with each *Flt3* shRNA was significantly reduced compared with the control shRNA-introduced MLL–AF9/Hes1$^{-/-}$ cells (Figure 5e). We further established *Flt3* knockout cell lines by using the CRISPR/CAS9 technology. We evaluated five independent clones with the *Flt3* genome edited, accompanying robust reduction of FLT3 expression (Figure 5f). Each *Flt3*-edited clone showed significantly reduced growth compared with the clone retaining *Flt3* genome and expression retained (Figure 5g).

Hes1 loss increases the frequency of leukemia-initiating cells

Based on the increase in the FLT3-positive cell frequency in MLL–AF9/*Hes1*$^{-/-}$ AML cells, we performed secondary transplantation by infusing serially diluted FLT3-positive or -negative MLL–AF9/*Hes1*$^{-/-}$ AML cells prepared from the primary mice. Although the mice transplanted with 10 000 FLT3-positive cells developed leukemia in the same latency as those transplanted with FLT3-negative cells, the mice transplanted with 1000 or 100 FLT3-positive cells developed leukemia in significantly shorter latencies than those transplanted with the same number of FLT3-negative cells (Figure 6). These data indicate that the FLT3-positive fraction contains leukemia-initiating cells at a greater frequency than the FLT3-negative fraction, consequently suggesting that loss of *Hes1* increases the number of leukemia-initiating cells.

Expression of *FLT3* mRNA is negatively correlated with that of *HES1* or *NOTCH2* in AML patient samples

We next assessed databases containing mRNA expression profiles derived from microarray analysis of 285 AML patient samples (www.ncbi.nlm.nih.gov/geo, accession number GSE1159; ref. 36) and found that 13 samples exhibited MLL fusions. In these